A Novel Electron Paramagnetic Resonance Phenomenon in a Barium Stronium Titanate Ceramic

Da-Yong Lu[1,a] and Xiu-Yun Sun[1,b]

[1]Research Center for Materials Science and Engineering, Jilin Institute of Chemical Technology,

45 Chengde street, Jilin 132022, China

[a]cninjp11232000@yahoo.com, [b]sunxiuyun1989@163.com

Keywords: Barium Stronium Titanate, Dielectric properties, Point defects, EPR, *g*-tensor

Abstract. The electron paramagnetic resonance (EPR) technique was employed to investigate the point defects in barium strontium titanate ceramics. All samples showed a strong EPR signal with $g = 2.000$, which was indexed as intrinsic Ti-vacancy defects. In $(Ba_{0.85}Sr_{0.15})TiO_3$ ceramic, which showed a tetragonal symmetry and consisted of the crystallites with average size of ~ 220 nm, a novel EPR powder spectrum was observed - the *g*-factor of the $g = 2.000$ signal evolved into a *g*-tensor, and the two weak signals with $g_3 = \sim 2.6$ and $g_1 = \sim 1.6$ gradually shifted toward the $g_2 = 2.000$ signal and approached to each other with increasing temperature.

Introduction

Barium strontium titanate [BST - $(Ba_{1-x}Sr_x)TiO_3$] ceramic, which is a solid solution of $BaTiO_3$ and $SrTiO_3$, has been on the hot topic in the dielectric field owing to its high dielectric constant in the vicinity of room temperature [1-5]. Fu *et al* reported that BST ceramics sintered at $1320^{\circ}C$ for 2 h are tetragonal when $x < 0.35$, while are cubic when $x \geq 0.35$ [4]. BST consists of Ba^{2+}, Sr^{2+}, Ti^{4+}, and O^{2-} ions, all of which are EPR-silent non-Kramers ions. Therefore, EPR signals detected in BST originate from the point defects trapping electrons in the BST lattice.

To date EPR spectrum in BST has not been reported. In this work, the EPR spectra of the tetragonal and cubic BST ceramics were investigated to understand defect chemistry in BST. A novel EPR phenomenon never reported in $BaTiO_3$-based ceramics was provided and discussed in association with g-tensor.

Experimental Procedure

The initial materials were AR-grade $BaCO_3$, $SrCO_3$, and TiO_2. BST ceramics were prepared at $1350^{\circ}C$ for 2 h in air using a conventional cold-press ceramic technique [6] according to a formula $(Ba_{1-x}Sr_x)TiO_3$ ($x = 0.15, 0.25, 0.35$).

Powder X-ray diffraction (XRD) measurements were made at room temperature using an X-ray diffractometer (D8 Advance, Germany). Crystal structure was determined by MS Modeling (Accelry Inc.) and Cu $K\alpha_1$ radiation ($\lambda = 0.1540562$ nm), as described elsewhere [7].

The surfaces of polished ceramic disks (0.8 mm in thickness) were sputtered with thin Au atoms and then pasted with silver to form electrodes for dielectric measurements. The temperature dependence of the dielectric constant was measured with a weak 1 kHz ac electric field using a RCL meter (Fluke PM6306, USA).

Atomic force microscopy (AFM) images were recorded in ambient environment using a CSPM-5000 scanning probe microscope system (Beyuan Nano-instruments Co., China) to scan the surface morphology of all samples. Scanning was carried out in contact mode AFM with a W-type silicon cantilever. The scanning frequency was set at 1.5 Hz.

Electron paramagnetic resonance (EPR) measurements for 30 mg of each powder sample were performed on a JES-RE3X spectrometer (JEOL, Japan) at X-band frequency (9.148 GHz), using microwave power of 4 mW and frequency modulation of 100 kHz. Before EPR measurements, each powder sample was heat-treated at $500^{\circ}C$ for 2 h. The *g*-value of ESR signal was calculated in terms of the 3rd and 4th lines of a standard Mn^{2+}/MgO sextet marker ($g_3 = 2.0327$ and $g_4 = 1.9810$).

Results and Discussion

The powder XRD patterns for $(Ba_{1-x}Sr_x)TiO_3$ ($x = 0.15, 0.25, 0.35$) ceramics are shown in Fig. 1. For simplicity, the three samples are denoted as BS15T, BS25T, and BS35T, respectively. BS15T and BS20T show a tetragonal perovskite structure. The lattice parameters (a, c) and unit cell volume (V_0) are $a = 3.9793$ Å, $c = 4.0091$ Å, $V_0 = 63.48$ Å^3 for BS15T and $a = 3.9738$ Å, $c = 3.9948$ Å, $V_0 = 63.08$ Å^3 for BS25T, respectively. BS35T has a cubic structure ($a = 3.9674$ Å, $V_0 = 62.45$ Å^3), in good agreement with the result reported by Fu et al [4].
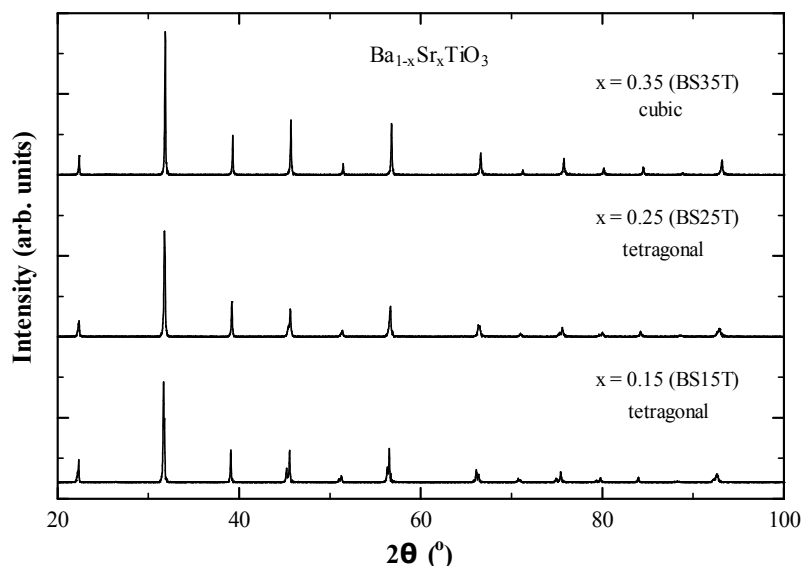
Fig. 1. Room-temperature XRD spectra of BST ceramic powders, (a) BS15T; (b) BS25T; (c) BS35T

In this work, the specimens for EPR measurements are from the ceramic powders, which were obtained by crushing and grinding the ceramic samples. In order to investigate the magnitude of ceramic crystallites, AFM was employed to observe the surface morphology of all samples, as shown in Fig. 2. A great deal of crystallites aggregates to form a bigger grain. The size distribution range of crystallites is 170~260 nm. The average size of crystallites for all ceramic samples is 220 nm, which can be regarded as the average size of the powders for EPR measurements.
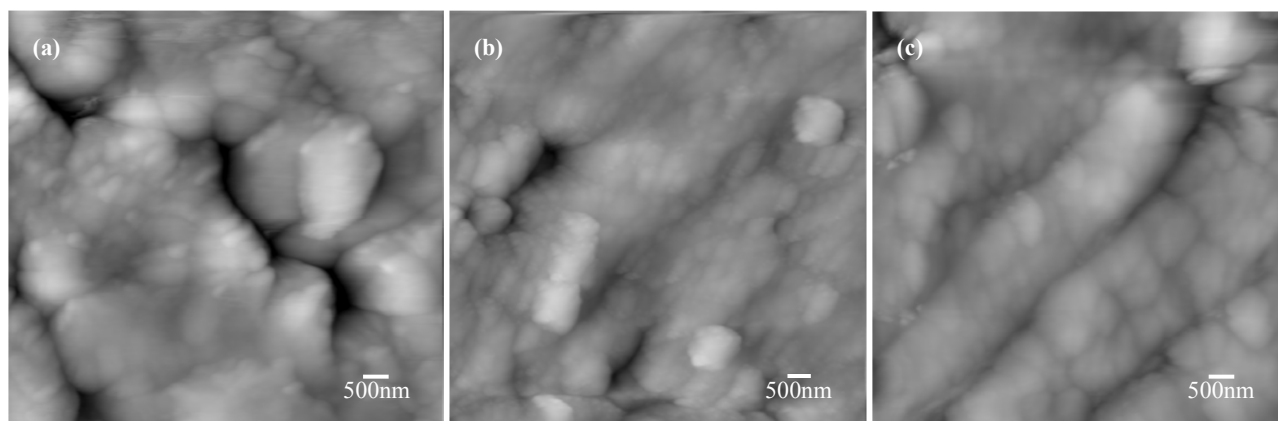
Fig. 2. AFM micrographs of polished BST ceramics, (a) BS15T; (b) BS20T; (c) BS35T

Room-temperature EPR spectra for the specimens are shown in Fig. 3. For all samples, a strong and symmetric EPR signal appears at $g = 2.000$. This signal is assigned to Ti-vacancy defects trapping electrons [8-12], which are the intrinsic defects formed in the lattice when the BST solid solution sintered was cooled to room temperature. A novel spectrum phenomenon occurs in the tetragonal BS15T, i.e., a pair of weak signals A and B appear on both sides of the $g = 2.000$ signal, while it was not observed in the tetragonal BS25T and the cubic BS35T. It is well known that the impurities Fe,

Mn, Cr, and Co are usually present in $BaTiO_3$ ceramics. However, we did not detect characteristic EPR signals associated with Fe^{3+} [13-15], Mn^{2+} [16], Cr^{3+} [17], and Co^{3+} [17]. Thus, the pair of signals is from neither the impurities nor other point defects.
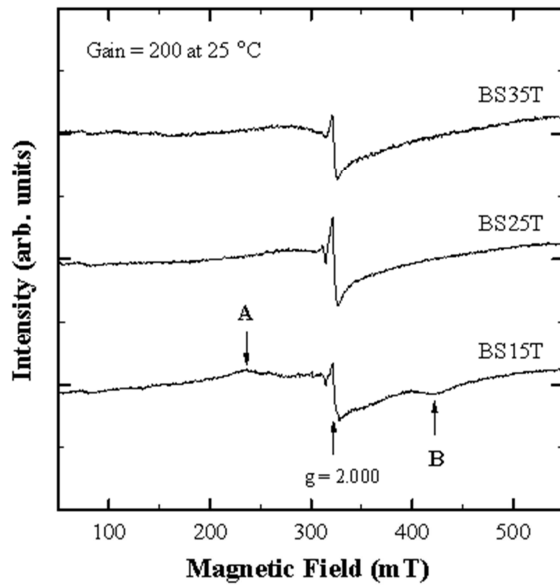
Fig. 3. EPR spectra of BST ceramic powders, measured at room temperature
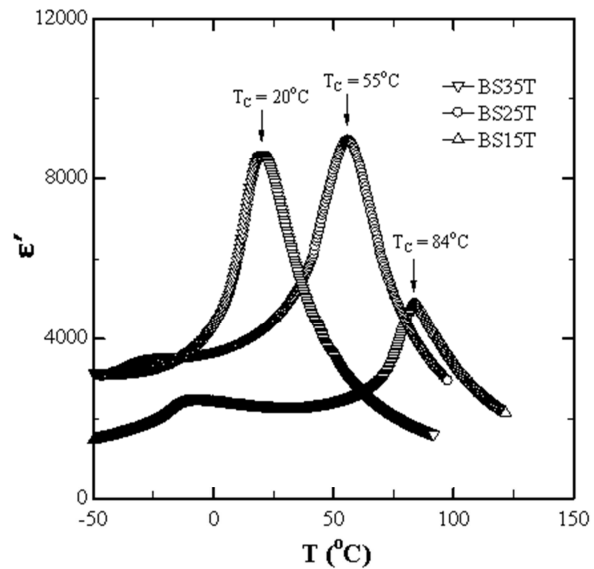
Fig. 4. Temperature-dependent dielectric constant for BST ceramics
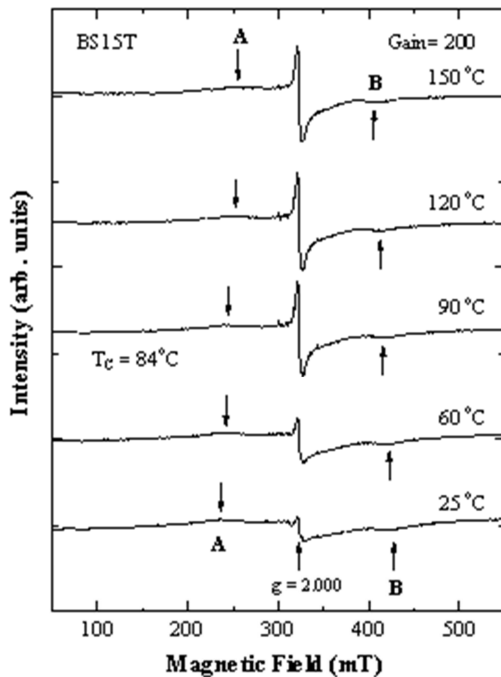
Fig. 5. EPR spectra of BS15T ceramic powders at different temperatures
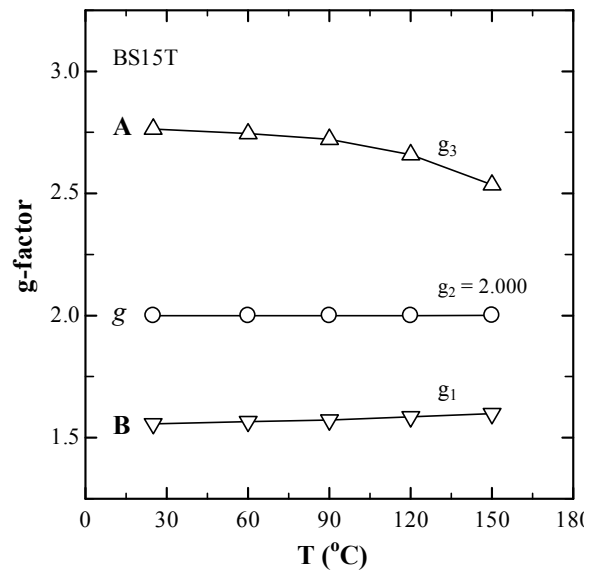
Fig. 6. Variation of the principle components of rhombic g-tensor, g_1, g_2, and g_3, as a function of temperature for BS15T. The circles represent the g_2 value corresponding to the strong signals at $g = 2.000$

It is well known that the $g = 2.000$ signal is activated above the Curie temperature (T_C) of $BaTiO_3$ [12]. In order to investigate the evolution of the pair of weak signals A and B with temperature, first of all, the temperature dependence of the dielectric constant for BST was measured for seeking for T_C, as shown in Fig. 4. The T_C value of BS15T is $84\,^{\circ}C$, and T_C decreases with increasing Sr content.

Fig. 5 shows EPR spectra of BS15T above room temperature. When $T > T_C (= 84\,^{\circ}C)$, the activation of the $g = 2.000$ signal is observed. On both sides of the $g = 2.002$ signal, the two signals at $g = \sim 2.6$ and ~ 1.6 gradually approach to each other with increasing temperature. Their variation in the g value with temperature is described in Fig. 6.

EPR signal may change with the storage history or heat treatment of specimen. The novel pair of lines in BS15T should originate from a thermally accessible spectrum induced by its storage history, the crushing extent of crystallites, and heat treatment at 500°C. The g values of the pair of lines are denoted as g_3 and g_1 (Fig. 6), forming an approximately centrosymmetric pattern around $g_2 = 2.000$.

The $g = 2.000$ signal arises from Ti-vacancy defects. In a thermally accessible spectrum, the g-factor of this signal evolves into a g-tensor, the formation of which is described in Fig. 7. When the g-tensor is rhombic and the principal components are well separated the powder spectrum is more structured [18]. Fig. 7a represents a realistic absorption spectrum including a finite linewidth on both sides of the main signal, which shows the low-field and high-field features. The two features correspond to the two g-tensor elements on both sides of the maximum $g_2 = 2.000$, respectively, because EPR signal observed is a first derivative spectrum, as shown in Fig. 7b. The maximum corresponds to the intermediate tensor element g_2.
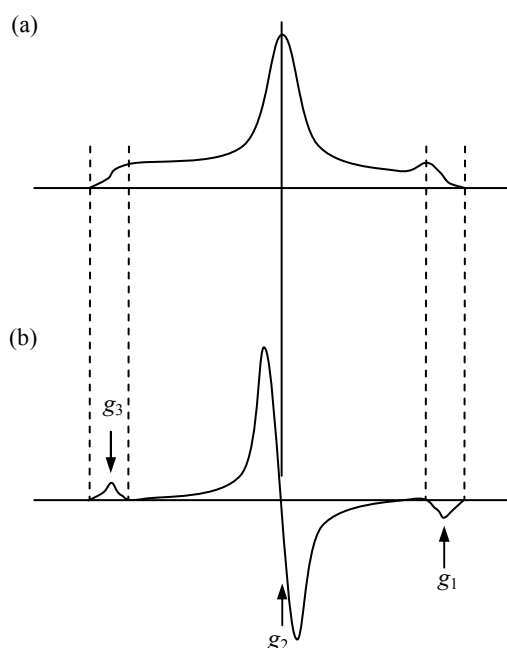
Fig. 7. First derivative powder spectrum for BS15T system having a rhombic g-tensor, $g_1 < g_2 < g_3$: (a) absorption spectrum including a finite linewidth, (b) the first derivative spectrum

Conclusions

The EPR technique was employed to investigate the point defects in $(Ba_{1-x}Sr_x)TiO_3$ ceramics. All samples show a strong EPR signal with $g = 2.000$, which is indexed as intrinsic Ti-vacancy defects. No signal associated with the impurities was detected. In the sample with x = 0.15, the g-factor of the $g = 2.000$ signal evolves into a g-tensor, accompanied by the two weak signals with $g_3 = \sim 2.6$ and $g_1 = \sim 1.6$, which gradually approach to each other with increasing temperature.

Acknowledgements

References

[1] A.B. Catalan, J.V. Mantese, A.L. Micheli, N.W. Schubring, and R.J. Poisson: J. Appl. Phys., Vol. 76 (1994), p. 2541

[2] D.M. Tahan, A. Safari, and L.C. Klein: J. Am. Ceram. Soc., Vol. 79 (1996), p. 1593

[3] S.C. Roy, M.C. Bhatnagar, G.L. Sharma, R. Manchanda, and V.R. Balakrishnan: Ceram. Int. Vol. 30 (2004), p. 2283

[4] C. Fu, C. Yang, H. Chen, Y. Wang, and L. Hu: Mat. Sci. Eng. B Vol.119 (2005), p.185

[5] C. Berbecaru, H.V. Alexandru, C. Porosnicu, A. Velea, A. Ioachim, L. Nedelcu, and M. Toacsan: Thin Solid Films Vol. 516 (2008), p. 8210

[6] D.-Y. Lu, M. Sugano, and M. Toda, J. Am. Ceram. Soc. Vol. 89 (2006), p. 3112

[7] D.-Y Lu, M. Sugano, W.-H Su, and T. Koda, Cryst. Res. Tech. Vol. 40 (2005), p. 703

[8] T. Kolodiazhnyi and A. Petric: J. Phys. Chem. Solids Vol. 64 (2003), p. 953

[9] T.D. Dunber, W.L. Warren, B.A. Tuttle, C.A. Randall, and T. Tsur: J. Phys. Chem. B Vol. 108 (2004), p. 908

[10] D.-Y Lu, X.-Y. Sun, and M. Toda: Jpn. J. Appl. Phys. Vol. 45 (2006), p. 8782

[11] D.-Y Lu, X.-Y. Sun, and M. Toda: J. Phys. Chem. Solids Vol. 68 (2007), p. 650

[12] D.-Y Lu, M. Toda, T. Ogata, and X.-Y. Sun: Jpn. J. Appl. Phys. Vol. 48 (2009), p. 021401

[13] T.R.N. Kutty, P. Murugaraj, and N.S. Gajbhiye: Mater. Lett. Vol. 2 (1984), p. 396

[14] E. Possenriede, O.F. Schirmer, and H.J. Donnerberg: Ferroelectrics Vol. 92 (1989), p. 245

[15] P. Murugaraj and T.R.N. Kutty: J. Mater. Sci. Lett. Vol. 5 (1986), p. 171

[16] H. Ikushima and S. Mayakawa: J. Phys. Soc. Jpn. Vol. 19 (1964), p. 1986

[17] R.N. Schwartz and B.A. Wechsler: Phys. Rev. B Vol. 48 (1993), p. 7057

[18] N.M. Atherton, *Principles of Electron Spin Resonance* (PEllis Horwood Limitted, England 1993).